Ultra-Large Field-of-View Retinal Projection Display with Vision Correction

Wenbo Zhang, Yuhang Wu, Lantian Mi, Chao Ping Chen, Lin Zhong, Bing Yu, Yang Li, and Nizamuddin Maitlo*

Smart Display Lab, Department of Electronic Engineering, Shanghai Jiao Tong University, Shanghai, China

Email: ccp@sjtu.edu.cn

Abstract

We propose a retinal projection display that is able to merge with vision correction. Our solution is highlighted by a corrective lens coated with an array of tiled organic light-emitting diodes and a transmissive spatial light modulator. Its design rules are set forth in detail, followed by results and discussion.

Keywords

augmented reality; near-eye display; retinal projection; field of view; vision correction.

1. Introduction

Today, the ultimate solution for a see-through near-eye display (NED) that would perfectly live up to the standards of augmented reality is still an open question. As far as the cost of fabrication is concerned, combiner-based NEDs [1-3] are preferred. However, due to the size of beam splitters and semi-reflective mirrors, such NEDs—if designed with a large field of view (FOV)—are often bulky and heavy. As far as the form factor is concerned, waveguide-based NEDs, including both planar [4-6] and freeform [7-9] waveguides, are favorable as the optical path can be compressed into the waveguide. However, once the light enters into a waveguide, the maximum angle, at which it could leave, will be bound by the total internal reflection and the ways of out-coupling. For this reason, FOVs of such NEDs are usually below 50° [10]. As far as FOV is concerned, retinal-projection-based NEDs [11-13] are unparalleled by the former two. For wearable NEDs, optics aside, ergonomics needs to be taken into account as well. One of the ergonomic pain points to solve is to save the visually impaired users from the trouble of wearing extra eyeglasses or contact lens. In this paper, a retinal-projection-based NED—we shall refer to it as retinal projection display (RPD) hereafter—that enables vision correction is proposed.

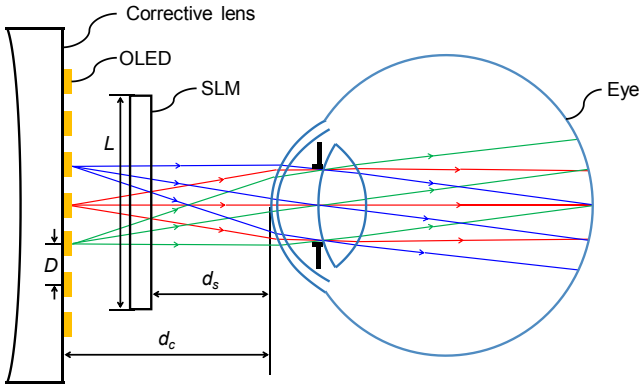

Figure 1. Schematic drawing of the proposed RPD.

2. Proposed Structure

Fig. 1 is the schematic drawing of the proposed RPD, which involves four major components, *i.e.* a corrective lens, an array of organic light-emitting diodes (OLEDs) [14], a transmissive spatial light modulator (SLM), and an eye. The corrective lens is used for compensating the refractive anomalies of the eye, say myopia. Preferably, its outer surface is concave, while its inner surface is flat, upon which OLEDs can be easily fabricated or laminated. OLEDs serve as the light source to illuminate the virtual image. Since the size of an individual OLED is way smaller than that of SLM, each OLED can be regarded as a point light source. The SLM is used for generating virtual images. d_s is the distance between the SLM and eye. d_c is the distance between the corrective lens and eye. D is the center spacing between two adjacent OLEDs. L is the dimension of SLM.

3. Principle

Design Rules: The design of the proposed RPD deals with two optical paths, one for imaging the real objects and the other for imaging the virtual objects. For the real image, as shown in Fig. 2, where both SLM and OLEDs are supposed to be transparent, light rays emitting from the real object will be first diverged by the corrective lens, and then converged by the eye. Through the accommodation of eye and the compensation of corrective lens, a clear image will be maintained on the retina as long as the real object is within the range of accommodation.

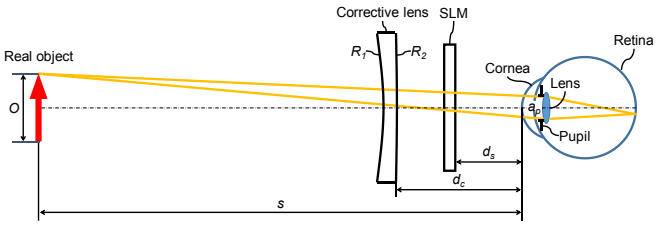

Figure 2. The optical path diagram for imaging the real object.

For the virtual image, as shown in Fig. 3, let us first consider a scenario when merely a single OLED is turned on. Light rays emitting from the OLED will first encounter the SLM and illuminate its pixels, which in turn form a real object A that is composed of the actual rays (solid lines). SLM is placed out of the range of accommodation. Therefore, instead of seeing the real object A, eye will trace back along the extended virtual rays (dashed lines) to see a virtual object S being formed at a distance s determined by Eq. (1)

$$s = \frac{s'}{(P_e+P)s'-1} \tag{1}$$

where P_e is the diopter of eye, P the diopter of the corrective lens, and s' the image distance. This implies that the object distance s could be adjusted by the eye. This phenomenon would be very

helpful for the image registration [2]—the alignment between the virtual and real objects—even without resorting to any zoom lens. By invoking the theorem of similar triangles, the size O of the virtual object can be easily deduced as

$$O = a_s\left(\frac{s-d_c}{d_c-d_s}\right) \tag{2}$$

where a_s is the size of unseen real object A. Similarly, we could also have

$$a_s = a_p\left(\frac{d_c-d_s}{d_c}\right) \tag{3}$$

where a_p is the pupil size, a brightness-sensitive variable. Normally, the pupil size of an adult varies from 2 to 4 mm in diameter in the bright ambience, whereas from 4 to 8 mm in the dark ambience [13]. To compromise between the bright and dark, pupil size of 4 mm is assumed hereafter. By substituting Eqs. (1) and (3) into Eq. (2), we have

$$O = a_p\left(\frac{s'}{(P_e+P)s'-1)d_c}-1\right) \tag{4}$$

from which it can be said that the size of virtual object largely hinges on the pupil size and diopter of eye. FOV of a single OLED, θ—defined as the angular extent of the virtual object—can be calculated as

$$\theta = 2tan^{-1}\left(\frac{O}{2s}\right) \tag{5}$$

Given s = 3 m, P_e= 43.15 m^{-1}, P= −2 m^{-1}, s'= 24.5 mm, a_p = 4 mm, d_c= 20 mm and, θ is only 11.3°. For θ= 100°, d_c shall be decreased to 1.68 mm, which is apparently impract ical. Hence, a tilted configuration with a multiple of OLEDs is required to achieve large FOV.

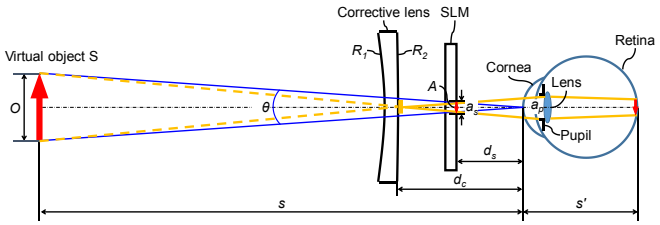

Figure 3. The optical path diagram for imaging the virtual object, when merely a single OLED is turned on.

Now consider a scenario when two adjacent OLEDs are simultaneously turned on, as illustrated in Fig. 4. There will be two virtual objects being imaged at the distance s. In order for these two virtual objects to be seamlessly tiled, the centers of two adjacent OLEDs should be spaced at an optimal distance D that is given by [13]

$$D = a_p\left(1-\frac{d_c}{s}\right) \tag{6}$$

where a_p is the pupil size, and d_c is the distance between the corrective lens and eye. The distance d_s between the SLM and eye should be adjusted as

$$d_s = \frac{a_p d_c}{a_p+D} \tag{7}$$

As can be inferred from Eq. (6), the optimal distance D will be subject to change as both pupil and diopter of eye may vary from time to time. When pupil expands or shrinks, shifting the pupil size away from the predetermined value, there will be an overlapping or gap between the neighboring virtual objects. To handle the change in pupil size, the array of tiled OLEDs shall be addressed in a way that it is able to dynamically tune the distance D to match with the current pupil size [13]. Since the distance d_c is usually way smaller than the object distance s, the change in diopter of eye, on the other hand, barely affects the distance D unless the object distance s becomes very close.

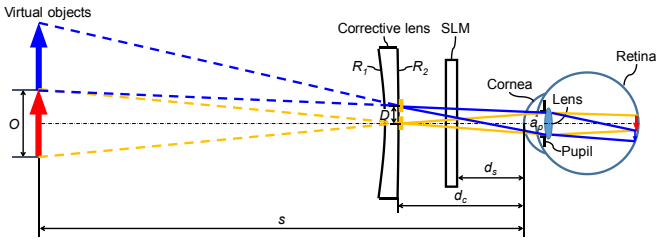

Figure 4. The optical path diagrams for imaging multiple virtual objects, when two adjacent OLEDs are simultaneously turned on.

Field of View: Referring to Fig. 5, FOV of the real image, FOV_r—defined as the angular extent of the corrective lens—can be calculated as

$$FOV_r = 2tan^{-1}\left(\frac{\sqrt{W^2+H^2}}{2d_c}\right) \tag{8}$$

where W and H represent the horizontal and vertical dimensions of the corrective lens, respectively. It can be seen that FOV_r is limited by the size of corrective lens and it would become larger as the eye gets closer to the corrective lens. On the other hand, FOV of the virtual image, FOV_v, is defined as the angular extent of the SLM—if SLM is fully illuminated and smaller than the corrective lens—which can be estimated with

$$FOV_v = 2tan^{-1}\left(\frac{L}{2d_s}\right) \tag{9}$$

where L is the dimension of SLM, measured in a given direction. Compared to FOV of a single OLED, FOV_v of tiled OLEDs has a simpler form that only involves the size of SLM and the distance d_s between the SLM and eye.

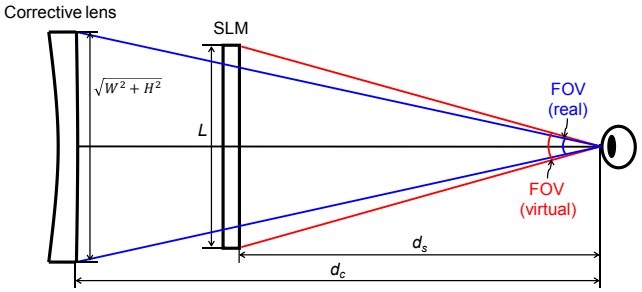

Figure 5. Definition of FOVs for both real and virtual images.

4. Results and Discussion

Simulation Settings: Our simulation is implemented with the optical design software Code V (Synopsys) to analyze the imaging properties, including modulation transfer function (MTF), distortion, and imaging simulation. Our design wavelength is 550 nm. Although a configuration with tiled OLEDs is proposed, our simulation is limited to the case of a single OLED. This is because it is technically impossible to set up more than one object in Code V. As the sharpest or best vision

occurs at the center of retina, where the fovea is located, a configuration with a single OLED being center-aligned with retina is adopted for the simulation. To avoid duplicate simulations, other cases are omitted.

The numbering of surfaces is labelled as in Fig. 6. The object represents either the real or virtual object that is 3 m away from the eye. Surfaces 1 to 2 (S1 to S2) make up the corrective lens. Surfaces 3 to 7 (S3 to S7) make up the eye, of which, S3 is anterior cornea, S4 is posterior cornea, S5 is anterior lens with pupil, S6 is posterior lens, and S7 is retina. In calculating the real image, all surfaces are active. In calculating the virtual image, surfaces 2 to 7 are active, while S1 is inactive. To treat the OLED, which is situated on S2, as a point light source, the semi-aperture of S2 is decreased to 0.1 mm.

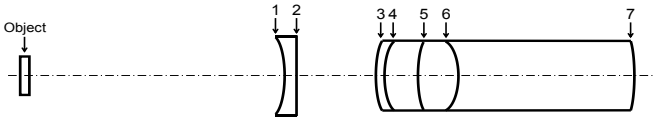

Figure 6. The numbering of surfaces.

According to the said design rules, we could create an initial structure by presetting the parameters for each element. Then, an optimization is carried out by constraining the effective focal length of the eye to be 24.5 mm—*i.e.* length of eye ball. The parameters obtained after the optimization are summarized in Table 1. Besides, more detailed parameters for defining aspherical surfaces are disclosed in Table 2.

Table 1. Parameters used for the simulation

Surface	Surface type	Radius (mm)	Thickness (mm)	Refractive index[a]	Semi-aperture (mm)
object	sphere	infinity	2978 / 2980[b]		
1	asphere	−294.8000	2	1.5896	4.5145
2	sphere	infinity	20		4.4012 / 0.1000[c]
3	asphere	6.6624	0.5000	1.3760	2.5790
4	asphere	3.5491	3.1600	1.3360	2.4065
5	asphere	11.4085	3.6000	1.4085	2.0000
6	asphere	−5.5801	17.2000	1.3360	1.9972
7	sphere	−11.0000	0.0000	1.3360	1.6144

[a]Refractive index is left empty when the medium is air. [b]Thickness of object is 2978 and 2980 mm for calculating the real and virtual images, respectively. [c]Semi-aperture of S2 is 4.4012 and 0.1 mm for calculating the real and virtual images, respectively.

Table 2. Parameters for aspherical surfaces

Surface	Y radius (mm)	Conic constant	4th order coefficient	6th order coefficient	8th order coefficient
1	−294.8000	0	1.0878E-05	−6.5664E-07	9.8302E-09
3	6.6624	−0.1800	0.0002	0	0
4	3.5491	−0.6000	0.0040	0	0
5	11.4085	−0.9427	0.0005	−0.0002	−2.9563E-06
6	−5.5801	2.5161	0.0051	−0.0002	3.2283E-05

FOV: Table 3 lists the parameters necessary for evaluating FOV of the tiled configuration. From Eqs. (8) and (9), FOV_r and FOV_v are calculated as 114° (diagonal) and 117° (diagonal), respectively.

Table 3. Parameters for calculating FOVs

Type	Parameter	Value
FOV_r	W	54 mm
	H	29 mm
	d_c	20 mm
FOV_v	L	1.3 inch (33.02 mm)
	d_s	10.03 mm

MTF: MTF is the most comprehensive performance criterion for NEDs. Fig. 7 shows the MTFs of both real and virtual images, where black dotted lines the MTFs inclusive of diffraction, while other lines the MTFs exclusive of diffraction. Since the tiniest aperture in our RPD—*i.e.* the pixel of SLM—is 15 μm across, which is almost two orders of magnitude larger than the wavelength, the diffraction is negligible. Moreover, owing to the rotational symmetry, the marginal angle is set as 5.65°—half of FOV of single OLED. For the real image, MTFs for all angles are above 0.4 at 280 cycles/mm. For the virtual image, MTFs for all angles are above 0.4 at 120 cycles/mm.

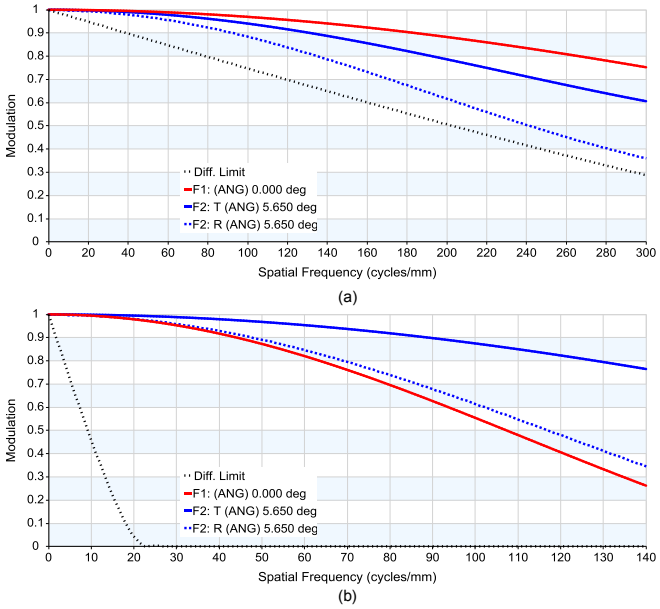

Figure 7. Calculated MTFs of (a) real and (b) virtual images.

Contrast Ratio: Contrast ratio (CR) is defined as the ratio of maximum intensity to minimum intensity, and it can be derived as [13]

$$CR = \frac{1+M\cdot MTF}{1-M\cdot MTF} \tag{10}$$

where M denotes the modulation in object, *i.e.*

$$M = \frac{CR_o-1}{CR_o+1} \tag{11}$$

where CR_o is the CR of object. For the real object, CR_o can be significantly large so that M is considered as 1. For the virtual object, CR_o is the CR of SLM. From Eqs. (10) and (11), for the spatial frequency of 33.33 cycles/mm—which corresponds to a pixel size of 15 μm—at the central angle, CRs of real and virtual images are calculated as 666 and 31, respectively.

Distortion: Distortion of real and virtual images, defined as the displacement of image height or ray location, are plotted in Figs. 8(a) and 8(b), respectively, where distortion of the real images is less than 0.04%, and distortion of the virtual images is less than 0.73%.

Simulated Imaging: For a qualitative analysis of imaging quality, both real and virtual images are visualized, as shown in Fig. 9. By comparing the original and simulated images, it can be seen that the real image is identical to the original one despite some chromatic aberration, while the virtual image turns out to be kind of blurred.

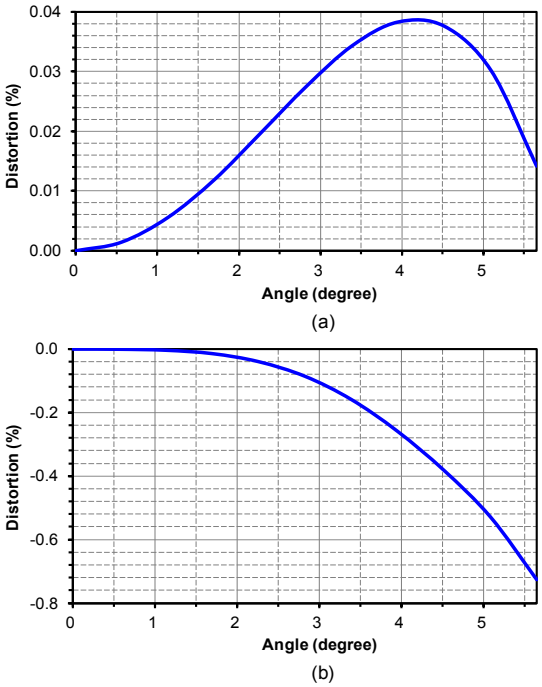

Figure 8. Calculated distortion of (a) real and (b) virtual images.

Figure 9. (a) Original, (b) real, and (c) virtual images.

5. Conclusions

A retinal-projection-based NED, also termed RPD, which enables vision correction is proposed. Its structure is highlighted by a corrective lens, an array of tiled OLEDs, and a transmissive SLM. Based on the simulation, its key performance including FOV, MTF, and distortion has been studied. For the real image, FOV is 114° (diagonal), MTF is above 0.4 at 280 cycles/mm, CR is 666, and distortion is less than 0.04 %. For the virtual image, FOV is 117° (diagonal), MTF is above 0.4 at 120 cycles/mm, CR is 31, and distortion is less than 0.73%.

6. Acknowledgements

Science and Technology Commission of Shanghai Municipality (1701H169200); Shanghai Jiao Tong University (AF0300204, WF101103001/085); Shanghai Rockers Inc. (15H100000157).

7. References

[1] S. Liu, H. Hua, and D. Cheng, "A novel prototype for an optical see-through head-mounted display with addressable focus cues," IEEE Trans. Vis. Comput. Graph. **16**(3), 381–393 (2010).

[2] Y.-J. Wang, P.-J. Chen, X. Liang, and Y.-H. Lin, "Augmented reality with image registration, vision correction and sunlight readability via liquid crystal devices," Sci. Rep. **7**, 433 (2017).

[3] L. Zhou, C. P. Chen, Y. Wu, Z. Zhang, K. Wang, B. Yu, and Y. Li, "See-through near-eye displays enabling vision correction," Opt. Express **25**(3), 2130–2142 (2017).

[4] Y. Amitai, "Extremely compact high-performance HMDs based on substrate-guided optical element," SID Symposium Digest of Technical Papers **35**, 310–313 (2004).

[5] T. Levola, "Diffractive optics for virtual reality displays," J. Soc. Inf. Disp. **14**(5), 467–475 (2006).

[6] H. Mukawa, K. Akutsu, I. Matsumura, S. Nakano, T. Yoshida, M. Kuwahara, and K. Aiki, "A full-color eyewear display using planar waveguides with reflection volume holograms," J. Soc. Inf. Disp. **17**(3), 185–193 (2009).

[7] X. Hu and H. Hua, "High-resolution optical see-through multi-focal-plane head-mounted display using freeform optics," Opt. Express **22**(11), 13896–13903 (2014).

[8] Y. Wu, C. P. Chen, L. Zhou, Y. Li, B. Yu, and H. Jin, "Design of see-through near-eye display for presbyopia," Opt. Express **25**(8), 8937–8949 (2017).

[9] Y. Wu, C. P. Chen, L. Zhou, Y. Li, B. Yu, and H. Jin, "Near-eye display for vision correction with large FOV," SID Symposium Digest of Technical Papers **48**, 767–770 (2017).

[10] O. Cakmakci and J. Rolland, "Head-worn displays: a review," J. Disp. Technol. **2**(3), 199–216 (2006).

[11] A. Maimone, D. Lanman, K. Rathinavel, K. Keller, D. Luebke, and H. Fuchs, "Pinlight displays: wide field of view augmented reality eyeglasses using defocused point light sources," ACM Trans. Graph. **33**(4), 89 (2014).

[12] M. Sugawara, M. Suzuki, and N. Miyauchi, "Retinal imaging laser eyewear with focus-free and augmented reality," SID Symposium Digest of Technical Papers **47**, 164–167 (2016).

[13] C. P. Chen, L. Zhou, J. Ge, Y. Wu, L. Mi, Y. Wu, B. Yu, and Y. Li, "Design of retinal projection displays enabling vision correction," Opt. Express **25**(23), 28223–28235 (2017).

[14] C. Chen, H. Li, Y. Zhang, C. Moon, W. Y. Kim, and C. G. Jhun, "Thin-film encapsulation for top-emitting organic light-emitting diode with inverted structure," Chin. Opt. Lett. **12**(2), 022301 (2014).